This work was carried out in whole or in part within the framework of the NOMATEN Centre of Excellence, supported from the European Union Horizon 2020 research and innovation program (Grant Agreement No. 857470) and from the European Regional Development Fund via the Foundation for Polish Science International Research Agenda PLUS program (Grant No. MAB PLUS/2018/8), and the Ministry of Science and Higher Education's initiative "Support for the Activities of Centers of Excellence Established in Poland under the Horizon 2020 Program" (agreement no. MEiN/2023/DIR/3795).

The version of record of this article, first published in Corrosion Science, Volume 238, September 2024, 112354, is available online at Publisher's website:
https://dx.doi.org/10.1016/j.corsci.2024.112354

Corrosion Science 238 (2024) 112354

Contents lists available at ScienceDirect

Corrosion Science

journal homepage: www.elsevier.com/locate/corsci

New insights into the corrosion of orthopedic Ti-6Al-4V under cathodic polarization

Agata Sotniczuk [a,b,*], Baojie Dou [c], Chenyang Xie [c], Junhui Tang [c], Damian Kalita [a], Witold Chromiński [a,b], Halina Garbacz [b], Fan Sun [c], Kevin Ogle [c,**]

[a] NOMATEN Centre of Excellence, National Centre for Nuclear Research, A. Sołtana 7, Otwock-Swierk 05-400, Poland
[b] Faculty of Materials Science and Engineering, Warsaw University of Technology, Woloska 141, Warsaw 02-507, Poland
[c] Chimie ParisTech, PSL University, CNRS, Institut de Recherche Chimie Paris (IRCP), F-75005, Paris, France

ARTICLE INFO

Keywords:
Titanium
Polarization
SEM
TEM
Interfaces
Passive films

ABSTRACT

This study offers a real-time monitoring of titanium dissolution in H_2O_2-enriched phosphate buffer solution (PBS) during polarization of Ti-6Al-4V at cathodic potentials using atomic emission spectroelectrochemistry (AESEC). Polarization had a deleterious effect on titanium dissolution when it was conducted at potentials between −0.5 V and −1 V. AESEC results demonstrate a non-linear and time-dependent relation between titanium dissolution and applied potential. Scanning and transmission electron microscopy (SEM) and (TEM) observations revealed that the vanadium-rich (β) phase is more sensitive to polarization-induced corrosion, which continues during subsequent Ti-6Al-4V exposure at open circuit potential.

1. Introduction

In the current orthopedic field, the Ti-6Al-4V alloy is a standard choice for the femoral stem component in total hip arthroplasty (THA) [1]. This material offers desirable mechanical performance along with confirmed biocompatibility, enabling successful osseointegration [2–4]. Ti-6Al-4V demonstrates spontaneous passivation resulting in the formation of a continuous nanometric titanium oxide film on its surface [5]. The oxide layer fully protects the Ti-6Al-4V alloy from corrosion in typical biological solutions, as specified by ASTM standards to simulate conditions near hip implants inserted into the human body [6,7]. However, previous literature studies have documented the possibility of implant corrosion *in vivo* [8,9], particularly within crevices at the metallic interfaces of modular hip replacements such as neck/stem or head/neck [10–13].

For hip replacements, one of the most aggressive conditions arises during mechanically assisted crevice corrosion (MACC) which is a combination of mechanical wear and crevice corrosion occurring simultaneously [14]. While the mechanical component of MACC has been widely studied and is relatively well described, understanding of the chemical processes involved in this phenomenon is still limited [11]. When the oxide layer formed on Ti-6Al-4V is disrupted due to mechanical abrasion, exposing the bare substrate to the solution, the oxide film immediately undergoes re-passivation owing to titanium's strong affinity to oxygen [15]. Re-passivation (oxidation reactions) results in the excessive generation of electrons at the metallic interface, which cannot be consumed by reduction reactions during the continuous abrasive process [11]. Consequently, during MACC, the electrochemical potential at the Ti-6Al-4V/fluid interface shifts in the cathodic direction, which has been confirmed by *in vitro* studies. It has been observed that Ti-6Al-4V abrasion in biological fluid can lead to decrease of potential value by up to −1 V [16]. However, the exact level of the potential excursion *in vivo* is not known which justifies testing corrosion of Ti-6Al-4V not only at −1 V but also at higher cathodic potentials that are closer to OCP [17–19].

Electrochemical experiments revealed that Ti-6Al-4V corrosion at cathodic potentials is accelerated especially in the presence of hydrogen peroxide which is one of the reactive oxygen species (ROS) generated by the immune cells [11,18,19]. ROS can be created during the initial post-inflammatory response as a physiological reaction of the human body to the invasive surgical procedure [20–22]. Moreover, the generation of ROS can be activated as a consequence of the release of metallic debris during MACC happening at the interfaces of implantable devices [23]. This justifies the necessity to verify corrosion resistance under

* Corresponding author at: NOMATEN Centre of Excellence, National Centre for Nuclear Research, A. Sołtana 7, Otwock-Swierk 05-400, Poland.
** Corresponding author.
E-mail addresses: agata.sotniczuk@ncbj.gov.pl (A. Sotniczuk), kevin.ogle@chimieparistech.psl.eu (K. Ogle).

https://doi.org/10.1016/j.corsci.2024.112354
Received 10 June 2024; Received in revised form 13 July 2024; Accepted 6 August 2024
Available online 8 August 2024

simultaneous presence of H_2O_2 and cathodic potentials.

To the date, effect of cathodic polarization on Ti-6Al-4V corrosion resistance was analyzed based on electrochemical techniques including new experimental approaches such as near-field electrochemical impedance spectroscopy (nEIS), which enables to get a rapid corrosion response [17]. Current works are focused also on incorporating experimental electrochemical data into deep neural networks to predict corrosion resistance [24]. Electrochemical measurements however cannot directly detect anodic reactions such as metal dissolution occur at rates considerably lower than the cathodic reactions. A direct measurement of metal dissolution during cathodic polarization is possible using atomic emission spectroelectrochemistry (AESEC) [25–28]. In this technique, the electrolyte, which is flowing and in contact with the tested sample, is transported continuously to an inductively coupled plasma atomic emission spectrometer (ICP-AES) directly during electrochemical test. In this way, real-time elemental dissolution may be measured directly [25]. Thereby, by utilizing AESEC technique, the objective of this study was to analyze Ti-6Al-4V dissolution rate in the conditions relevant for hip implants including cathodic polarization and the presence of inflammatory species in the fluid. Further understanding of the origin of corrosion response was possible by exploiting scanning and transmission electron microscopy. Specifically the following questions are addressed:

(i) How is the elemental dissolution rate of Ti-6Al-4V in H_2O_2-rich solution affected by the cathodic polarization which can happen during a MACC event?
(ii) How does the elemental dissolution depend on the value of applied cathodic potential and polarization time?
(iii) What do the Al-rich (α) and V-rich (β) phases differ in their sensitivity to dissolution and what surface changes correspond to corrosion process?

2. Materials and methods

2.1. Material preparation

The titanium alloy used in this research is known as Ti-6Al-4V (ASTM Grade 5) with (α+β) microstructure. Elemental composition of the alloy manufactured by Goodfellow meets ASTM B348 standard [29] and is provided in Table 1. According to technical sheet provided by manufacturer, mechanical properties of tested material are as follows: Tensile strength=895 MPa, Modulus of elasticity=106–114 GPa, Elongation to break>10 %. The alloy was cut into 20 mm diameter and 1 mm thickness discs and ground to #1200 grit and cleaned ultrasonically with ethanol and then with deionized water. For all of the samples this procedure was completed 15 minutes prior to use and prepared samples were stored in air before the test.

2.2. Solution preparation

Phosphate buffer saline (PBS) solution of pH 7.4 was prepared by dissolving a PBS tablet (Sigma-Aldrich, reference P4417) in 200 ml of deionized water (Milipore 18 MΩ) with final composition of 10 mM phosphate ($H_2PO_4^-$ + HPO_4^{2-}) buffer, 137 mM sodium chloride and 2.7 mM potassium chloride, at 25°C. The PBS electrolyte was used either alone or enriched with 33 mM H_2O_2 (PBS+H_2O_2) to simulate inflammatory conditions. The same concentration of H_2O_2 (33 mM) was used to test inflammatory-induced corrosion of Ti-6Al-4V in a previous study [20]. Although the concentration of H_2O_2 under physiological conditions typically reach μM level, locally it can be increased to the mM range [20]. The experiments were performed at room temperature (23℃) with natural aeration.

2.3. Dissolution rate analysis: AESEC study

The Ti-6Al-4V specimen served as the working electrode in a three-electrode AESEC electrochemical flow cell operating at a flow rate of 1 ml min^{-1} in conjunction with a saturated calomel reference electrode (SCE) and a Pt sheet counter electrode respectively. Details of the AESEC method and flow cell have been previously described [24]. Electrochemical conditions were controlled with a Gamry Reference 600 potentiostat/galvanostat. Electrochemical tests were performed in a potentiodynamic and potentiostatic modes. Experiments in potentiodynamic mode were conducted from the open circuit potential (OCP) up to −1.5 V vs. SCE with a scan rate 1 mV/s. Tests in potentiostatic mode were carried out for 20 minutes at the following potentials: (i) −0.25 V vs. SCE, (ii) −0.35 V vs. SCE, (iii) −0.5 V vs. SCE, (iv) −0.75 V vs. SCE, (v) −1 V vs. SCE. OCP was monitored for 20 minutes before and after all of polarization experiments. The concentrations of dissolved ions released from the Ti-6Al-4V specimen were monitored in real time using a downstream inductively coupled plasma atomic emission spectrometer (ICP-AES) (Horiba Ultima 2C) calibrated using standard methodology. The dissolution rates of the elements were calculated from the signal intensity based on equations presented previously [25]. Detection limits for Ti, Al and V under the conditions of these experiments were as follows: (i) Ti: 0.002 ppm, (ii) Al: 1.53 ppm and (iii) V: 0.005 ppm based on the equivalent concentration of the 3x the standard deviation of the blank (3σ).

2.4. Surface characterization: SEM and TEM studies

Although increased Ti-6Al-4V dissolution was detectable during AESEC tests in PBS+33 mM H_2O_2, virtually no signs of corrosion were observed by microscopy after a single cathodic polarization event in this solution. To accelerate the corrosion process, electrochemical experiments in the flowing system were performed additionally in PBS+100 mM H_2O_2 which allowed to visualize corrosion damages. The same concentration of H_2O_2 was used also in previous studies related to Ti-6Al-4V [19,30]. Finally, Ti-6Al-4V subjected to tests in flowing PBS+100 mM H_2O_2 was left in remaining solution for 72 h (3 days). This allowed to analyze differences in the oxide film thickness that was re-growth on Al-rich and V-rich phases after cathodic polarization. Top-view surface observations were performed with a scanning electron microscope: SEM (a Helios 5 UX DualBeam, Thermo Fisher Scientific). From Ti-6Al-4V after 3-days of immersion in PBS+100 mM H_2O_2, a thin foil was cut using FIB to visualize surface cross-section. Thin foil was characterized using a transmission electron microscope: TEM (a Jeol F200), with a special emphasize on the thickness and chemical composition of oxides formed on aluminum and vanadium-rich phases during Ti-6Al-4V immersion in simulated inflammatory fluid.

3. Results

3.1. Corrosion behavior under gradually decreasing cathodic potentials: AESEC studies

Fig. 1 gives the AESEC cathodic polarization curves of Ti-6Al-4V in PBS and PBS+H_2O_2 showing the electrochemical current (j_e) and the Ti dissolution current (j_{Ti}) on a log scale. The points on the curve represent

Table 1
Composition of Ti-6Al-4V in weight % (ASTM Grade 5, ASTM B348 chemistry only) alloy as supplied by Goodfellow.

N	C	H	O	Fe	Al	V	Ti	Other elements
max. 0.05	max. 0.08	max. 0.015	max. 0.20	max. 0.40	5.50–6.75	3.50–4.50	Bal.	max. 0.40

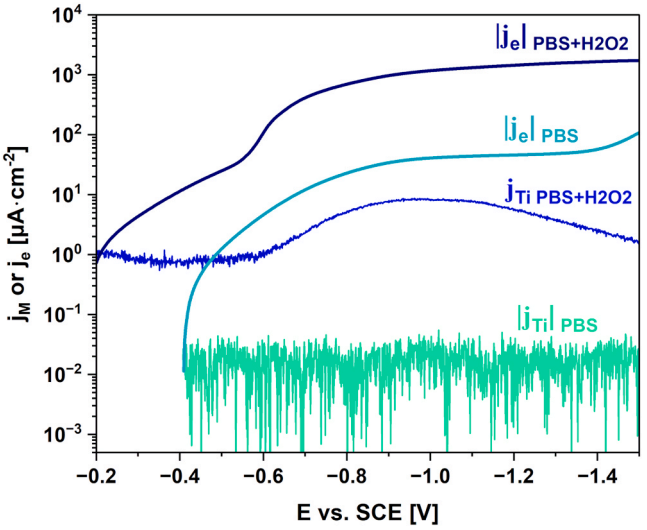

Fig. 1. Electrochemical $|j_e|$ and titanium dissolution $|j_{Ti}|$ current recorded during potentiodynamic polarization tests conducted from OCP up to −1.5 V vs. SCE in PBS or PBS+H_2O_2. Note variation of the |je| slope in PBS+H_2O_2, which correlates with the increase of j_{Ti}.

measurements from open circuit potential, which was around 200 mV higher in PBS+H_2O_2. Fig. 2 shows the results of the full experiment including the open circuit potential periods before and after polarization and includes the V dissolution rate (ν_V) as well.

The electrochemistry of the electrolyte is visible in the conventional polarization curve of j_e vs. E, as measured by the potentiostat. For PBS, a limiting current of approximately 30 μA was obtained consistent with a diffusion limited reduction of background oxygen (Eq. 1) by either the n=2 mechanism to form H_2O_2 or the n=4 mechanism to form OH^- directly [31]. The addition of H_2O_2 results in the appearance of a second

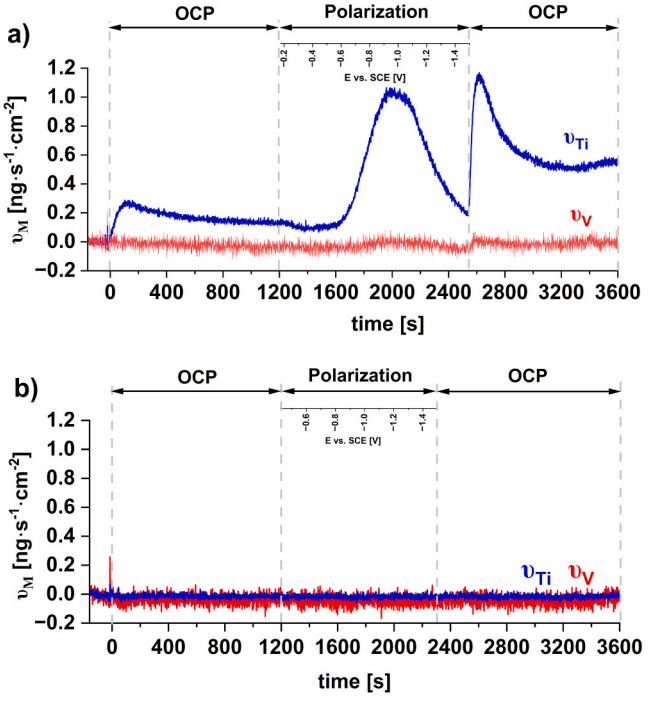

Fig. 2. Variations of potential and elemental dissolution rate (ν_M) registered in a) PBS+H_2O_2 and in b) standard PBS during OCP monitoring and potentiodynamic polarization towards cathodic direction. Note the detectable dissolution of titanium and vanadium in PBS+H_2O_2 and the lack of elemental dissolution in PBS.

reduction wave associated with H_2O_2 reduction (Eq. 2) with the cathodic current reaching a maximum around −1.7 mA·cm^{-2}. The Tafel slope decreased from 210 mV decade^{-1} for the first wave to 110 mV decade^{-1} for the second wave (Fig. 1).

$$O_2 + 2H_2O + 2e^- \rightarrow H_2O_2 + 2OH^- \quad (n = 2) \tag{1}$$

$$O_2 + 2H_2O + 4e^- \rightarrow 4OH^- \quad (n = 4)$$

$$H_2O_2 + 2e^- \rightarrow 2OH^- \tag{2}$$

The Ti dissolution rate measured throughout the polarization experiment demonstrates that the presence of H_2O_2 in the electrolyte was necessary to obtain a measurable Ti dissolution rate (ν_{Ti}). For the PBS electrolyte, Ti dissolution was not detected (<1 ml min^{-1} x 0.002 ppm) during the potential sweep or during the open circuit periods before and after the potential sweep (Fig. 2b). By contrast, for PBS+H_2O_2, significant Ti dissolution was detected throughout the experiment, at open circuit (Fig. 2) and during the cathodic potential sweep. Approximately 750 s of OCP monitoring in PBS+H_2O_2 were required to stabilize ν_{Ti} (Fig. 2a, Table 2). During the early stages of the potential sweep, ν_{Ti} decreased slightly from OCP to approx. −0.6 V (Fig. 2). For E > −0.6 V, ν_{Ti} increased to a maximum at −1.0 V (Fig. 2a, Table 2) and then decreased progressively until the end of the polarization test at −1.5 V (Fig. 2a). The onset of Ti dissolution corresponds approximately to the onset of the second wave of H_2O_2 reduction.

Interestingly, the highest ν_{Ti} was detected not during cathodic polarization but immediately after returning to the steady-state conditions (Fig. 2a, Table 2). Although ν_{Ti} dropped quickly and stabilized during the OCP measurement (see time > 2600 s in Fig. 2a), its value was still significantly greater than that registered before cathodic polarization (Table 2). This means that even a single excursion towards negative potentials enhanced the sensitivity of the Ti-6Al-4V alloy to H_2O_2-induced dissolution under steady-state conditions. Moreover, it suggests that cathodic polarization induced changes in the oxide layer which were not reversible during the time scale of this experiment. This may be due to the partial reduction of the oxide film according to the following reactions [32]:

$$TiO_2 + xH^+_{aq} + xe^- \leftrightarrow TiO_{2-x}(OH)_x \tag{3}$$

$$TiO_2 + 3H^+ + e^- \rightarrow Ti(OH)^{2+} + H_2O \tag{4}$$

The dissolution of V was also monitored during the experiment. A slight dissolution rate is observed rising moderately above the detection limit. It appears to follow closely the changes in the Ti dissolution rate. A more complete discussion of V dissolution will be given in the next section.

3.2. Corrosion behavior under fixed cathodic potentials: AESEC studies

During the abrasive process, the potential is expected to reach a particular negative value within seconds [16]. For this reason, analyzing the elemental dissolution during the application of a fixed cathodic potential (potentiostatic mode) may provide more a realistic approximation of the MACC situation. As no elemental dissolution was observed under potentiodynamic polarization in standard PBS solution, potentiostatic tests were performed only in PBS fluid enriched with H_2O_2 (Figs. 3–5). The imposed potentials were selected considering values that can be achieved *in vivo* (up to −1 V) [17].

The variation of the Ti dissolution rate (ν_{Ti}) as a function of time for different applied cathodic potentials are given in Fig. 3. The spontaneous corrosion rate (OCP) during the first 1200 s was similar for all experiments (Table 3). For the ensemble of experiments, the OCP dissolution rate of Ti (at time from 600 s to 1200 s) was 0.199 ng·s^{-1}·cm^{-2} ± 0.011 ng·s^{-1}·cm^{-2}. This indicates satisfactory repeatability of AESEC tests (Fig. 3). Polarization at the potentials with values closest to OCP (-0.25 V or −0.35 V) resulted in a slight decrease

Table 2
Dissolution rate and dissolution current calculated based on AESEC data registered at OCP and during Potentiodynamic Polarization scan conducted in PBS+H_2O_2 (j_{Ti} was calculated from ν_{Ti} applying Faraday's law).

	OCP	Potentiodynamic Polarization			OCP	
	t=600 s	-0.35 V	-1 V	-1.5 V	t=2620 s	t=3200 s
ν_{Ti} [ng·s^{-1}·cm^{-2}]	0.17	0.10	1.02	0.19	1.14	0.53
jTi [μA·cm^{-2}]	1.30	0.80	8.22	1.51	9.21	4.30

of ν_{Ti} which then returned to the previous OCP value immediately after the polarization (Fig. 3, Table 3). Moreover, for these polarization conditions, the dissolution current (j_{Ti}) provided important contribution to the overall electrochemical current ($|j_e|$) registered during polarization process (Fig. 4).

The Ti dissolution rate (ν_{Ti}), dissolution current (j_{Ti}) as well as electrochemical current ($|j_e|$) were significantly enhanced for polarizations of −0.5 V or below (Fig. 3, Fig. 4). For an Eap of −0.75 V ($|j_e|$ ≈0.66 mA·cm^{-2}) and −1.0 V ($|j_e|$ ≈1.05 mA·cm^{-2}). For these potentials values ($|j_e|$) are significantly greater compared to j_{Ti} (Fig. 4), which confirms that cathodic process at lower potentials is dominated by O_2 and H_2O_2 reduction. The dissolution profile (Fig. 3) shows two major kinetic events: a rapid dissolution which appears as a separate peak for the Eap = −1 V (a_1) and as a shoulder for the −0.5 V and −0.75 V (a_1) followed by a second peak (a_2). This time domain is highlighted by the expanded scale inset in Fig. 3. This was followed by a second and more intense maximum in the dissolution rate which reached a plateau and then decreased progressively.

When the system returned to the open circuit potential after polarization, the dissolution rate shot up once again, passed through a maximum and then slowly dropped towards the original OCP dissolution rate, although that rate was not obtained on the time scale of these experiments. For the Eap = −0.5 V ($|j_e|$ ≈ 0.2 mA·cm^{-2}), the Ti dissolution rate rose much more slowly and only started to decrease at the end of the experiment.

These results are consistent with a mechanism involving two independent reaction processes induced by the cathodic reaction. First, the cathodic potential and/or current induces changes in the oxide film that render it more susceptible to reaction with H_2O_2. These changes may involve the direct reduction of the oxide film leading to the appearance of the first dissolution event. Secondly, the cathodic potential reduces the concentration of H_2O_2 by reaction (Eq. 2) in the immediate surface vicinity. The result is that the dissolution rate initially increases with time but ultimately decreases as the electrolyte becomes less reactive. When the applied cathodic potential is removed, H_2O_2 would diffuse into the near surface region and the corrosion reaction would increase once again. Finally, the dissolution rate would decrease as the altered oxide material is dissolved and a new TiO_2 film is formed.

Simultaneously with monitoring of j_{Ti}, dissolution of vanadium (j_V) was registered as releasing of vanadium can induce neurotoxic effect and assessing the risk of this process is essential for the biomedical field (Fig. 5). Similarly to j_{Ti}, during cathodic polarization j_V achieved the largest value when test was carried out at −0.5 V (Fig. 5b). Maximum j_V was observed at the very close time point (around t=2100 s) as the maximum of j_{Ti} (Fig. 4, Fig. 5b). Considering j_{Ti} at this time point and Ti/V mass ratio in Ti-6Al-4V, it can be expected that j_V should be around 0.67 μA·cm^{-2}, while j_V was found to be almost twice as large (1.15 μA·cm^{-2}). This indicates slightly privileged dissolution of vanadium during cathodic polarization, which consequently suggests preferential degradation of beta phase. However, to confirm this finding and to get information about the extent of corrosion, AESEC studies were supplemented by surface characterization using microscopy techniques.

3.3. Surface evolution induced by cathodic polarization: SEM and TEM studies

AESEC experiments performed at fixed cathodic potentials revealed that the highest dissolution rate was achieved when Ti-6Al-4V was polarized at −0.5 V. However, top-view SEM analysis (Figs. 6–9) of the specimen surface did not reveal any significant changes following polarization at −0.5 V in PBS+33 mM H_2O_2 (Fig. 6a, b).

To observe corrosion damages that can be induced by short cathodic polarization at −0.5 V, electrochemical experiments in the flowing system were repeated in solution with higher H_2O_2 content (PBS+100 mM H_2O_2). The same H_2O_2 concentration was used in simulated inflammatory corrosion tests e.g. by Prestat et. al. [19] and Kurtz et. al. [11]. Similarly to tests performed in lower concentration of H_2O_2, no local corrosion damages such as pits and cracks were detected after polarization performed in PBS+100 mM H_2O_2 (Fig. 7a, c). However, differences in height of α and β grains indicate selective dissolution of β phase during cathodic potential excursion (Fig. 7a, c). Moreover, a sponge-like surface nanotopography, typical for H_2O_2-treated titanium materials, can be observed for grains of both α and β phases (Fig. 7a, c) [33].

SEM observations were repeated for Ti-6Al-4V which was subjected to polarization at −0.5 V and subsequently left in PBS+100 mM H_2O_2 for 72 h (Fig. 7b, d). This allowed to verify if selective dissolution of β phase, induced by single cathodic polarization event, was more pronounced when Ti-6Al-4V is further exposed to simulated inflammatory fluid at steady-state electrochemical conditions. It can be noticed that differences in topographical contrast between α and β phases are stronger after prolonged immersion of Ti-6Al-4V at OCP (Fig. 6, Fig. 7). This can be related to the progressive dissolution of β phase at steady-state conditions and/or preferential oxide film growth/re-deposition of corrosion products on grains of α phase.

These assumptions were verified by TEM observations of FIB lamella that was cut from the surface cross-section (Fig. 8). TEM observations revealed that differences between the height of α and β grains was around 19 nm. Moreover, differences were also found in the morphology and thickness of the oxide layer that was formed on the grains of α and β phases (Fig. 8). For β grain oxide film thickness was 17 nm, while for α grain the average oxide thickness was around 25 nm (Fig. 9). Considering these discrepancies, it can be concluded that for Ti-6Al-4V, the β-phase preferentially dissolved when exposed to the simulated inflammatory, H_2O_2-rich solution. For α-phase, oxide layer growth, rather than dissolution was favored. Moreover, it should be noticed that for both phases the outermost part of the oxide is enriched with Al.

4. Discussion

Ti-6Al-4V is prone to corrosion induced by ROS such as H_2O_2 that can be generated during post-surgery acute inflammatory reaction or as a further response of immunological system to releasing of implant's degradation products such as metallic debris. Previous analysis revealed that Ti-6Al-4V corrosion under inflammatory conditions can be facilitated under negative potential excursions, which can happen during mechanically assisted corrosion events [11,16,18,19]. Considering the fact that the interaction between biomaterial and immunological system creates a positive feedback loop since corrosion will induce inflammation and inflammation will induce corrosion [23], gaining the knowledge about Ti-6Al-4V dissolution during particular stages of electrochemical process is essential to understand and predict possible biological reactions that can happen *in vivo*.

AESEC experiments presented in this study respond to this

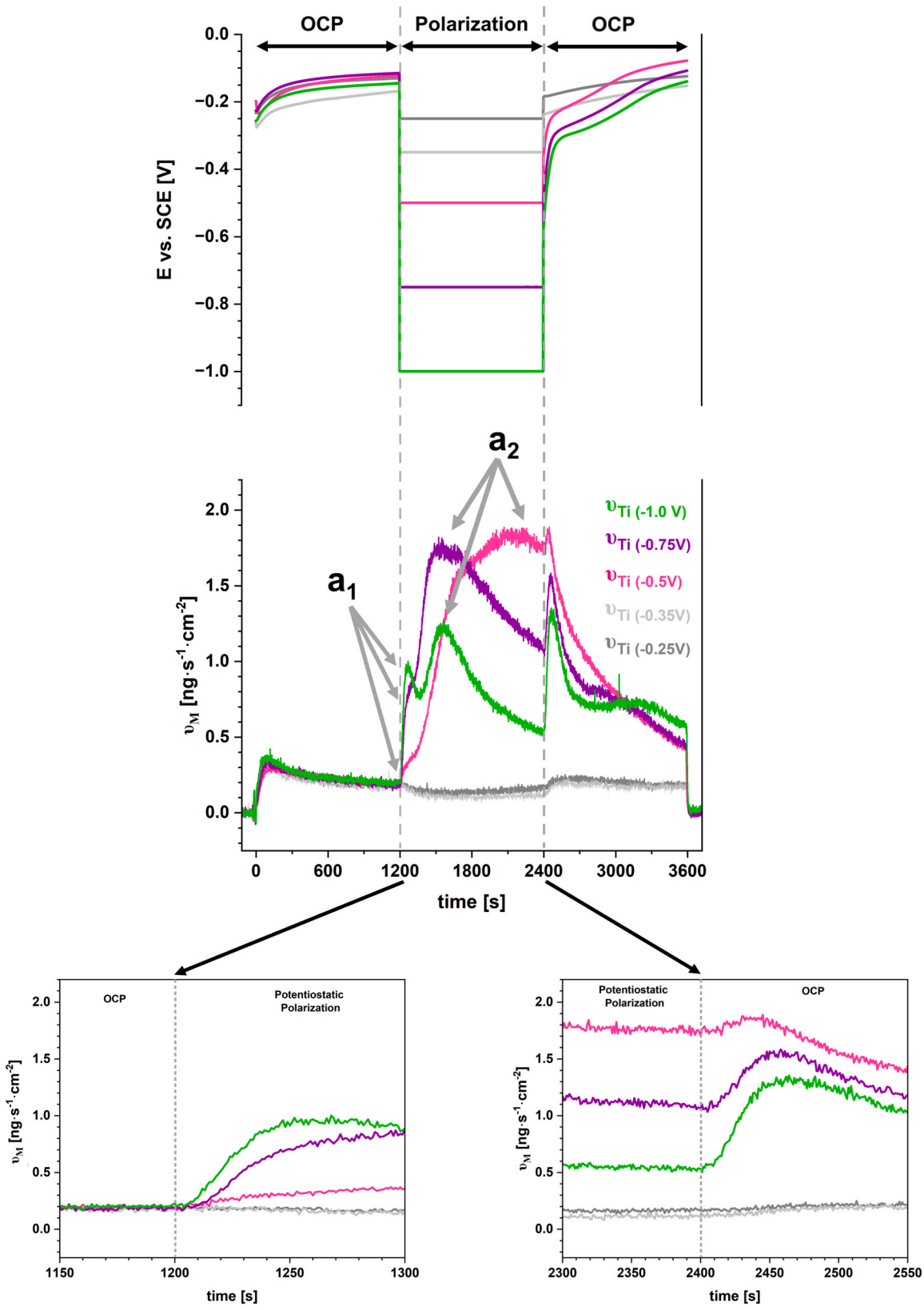

Fig. 3. Variations of potential and titanium dissolution (ν_{Ti}) in PBS+H_2O_2 during OCP monitoring and cathodic polarization at fixed potentials. Dissolution peaks detected during cathodic polarization (a_1 and a_2) are marked by arrows. Note the systematic variations of ν_{Ti} during polarization time when the value of applied potential was −0.5 V or below.

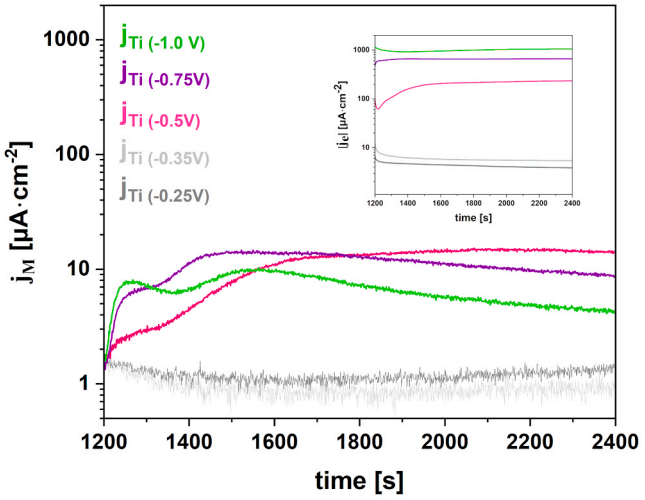

Fig. 4. Variation of j_{Ti} and $|j_e|$ registered in PBS+H_2O_2 during polarization in potentiostatic mode. Note that for potentials −0.5 V and below, j_{Ti} is many times lower compared to $|je|$.

requirement by offering the possibility of monitoring the elemental dissolution rates directly during particular stages of fully controlled electrochemical process. In this study we designed AESEC methodology that allowed us to gain knowledge about titanium and vanadium dissolution rates in the following situations: (i) at the steady-state conditions during initial contact of Ti-6Al-4V with simulated inflammatory fluid, (ii) during cathodic polarization under clinically relevant potential values, (iii) at the steady-state conditions after completing potential excursions. Overall results demonstrate that the titanium dissolution rate is significantly affected by cathodic polarization and depends on both the applied potential and/or the cathodic current and the polarization time. Performing polarization with negative potentials that were closest to OCP (-0.25 V or −0.35 V) resulted in a slight decrease of titanium dissolution rate (Table 3). The dissolution rates of Ti before and after polarization were nearly identical (Fig. 3). Small polarization towards negative directions should reduce Ti oxidation rate without lowering H_2O_2 concentration or damaging oxide film by increasing its defectiveness. These results follows findings presented by Kurtz et al. [34] who claim that cathodic polarization and H_2O_2 together accelerates corrosion of Ti-6Al-4V when applied potential value is lower than −0.3 V vs. Ag/AgCl (-0.345 V vs. SCE).

Titanium dissolution rate substantially increased when Ti-6Al-4V was polarized at −0.5 V or lower potentials (Fig. 3). Dissolved titanium can react with H_2O_2 according to Eq. 5 [35].

$$Ti(IV)_{aq} + H_2O_2 \rightarrow Ti(IV)O_2(OH)_{n-2}{}^{(4-n)+} + nH^+ \quad (5)$$

During first seconds of polarization as was expected the Ti dissolution rate increased more rapidly at the more negative potentials (Fig. 3, Table 3). This can be related to the most pronounced increase of oxide defectiveness, which could facilitate ion transport across the surface [34,

Table 3
Dissolution rate (ν_{Ti} [ng·s^{-1}·cm^{-2}]) and dissolution current (j_{Ti}[µA·cm^{-2}]) calculated based on AESEC data registered at OCP and during Potentiostatic Polarization scan conducted in PBS+H_2O_2 (j_{Ti} was calculated from ν_{Ti} applying Faraday's law).

	OCP (t=600 s)		Polarization (t=1250 s)		Polarization (t=2100 s)		OCP (t=2440 s)	
	ν_{Ti}	j_{Ti}	ν_{Ti}	j_{Ti}	ν_{Ti}	j_{Ti}	ν_{Ti}	j_{Ti}
−0.25 V	0.21	1.70	0.18	1.43	0.16	1.27	0.21	1.68
−0.35 V	0.20	1.59	0.17	1.35	0.11	0.87	0.16	1.24
−0.5 V	0.23	1.87	0.30	2.45	1.86	14.99	1.84	14.83
−0.75 V	0.21	1.71	0.71	5.70	1.28	10.32	1.49	12.05
−1 V	0.24	1.94	0.91	7.37	0.64	5.17	1.19	9.57

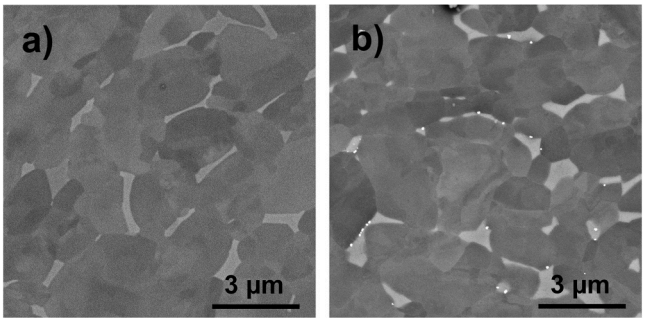

Fig. 6. Ti-6Al-4V surface a) in the polished state (outside tested area), b) after electrochemical tests in PBS+33 mM H_2O_2 performed according to following sequence: OCP (1200 s) –polarization at −0.5 V (1200 s) – OCP (1200 s). Vanadium-rich β phase is visible as brighter grains.

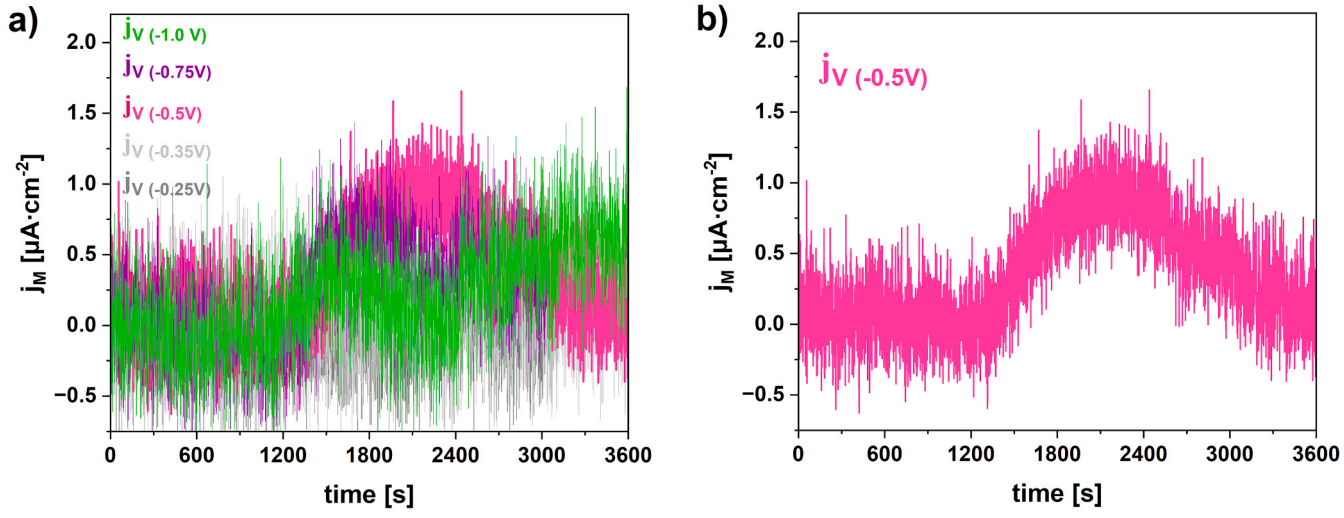

Fig. 5. Vanadium dissolution current (j_V) registered in PBS+H_2O_2 during OCP monitoring and polarization in potentiostatic mode: a) data registered for all fixed potentials, b) data for −0.5 V vs. SCE. Note the highest j_V detected during polarization at −0.5 V.

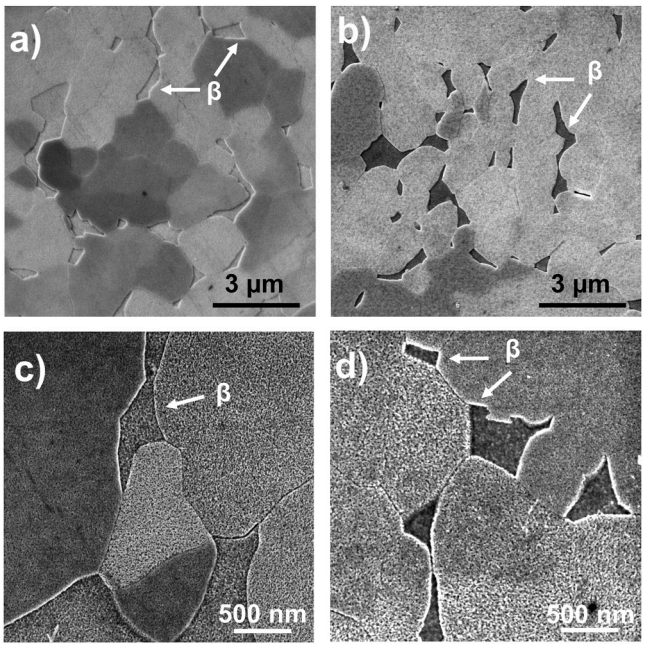

Fig. 7. SEM images of Ti-6Al-4V that visualize surface topography after electrochemical tests in PBS+100 mM H_2O_2 performed according to following sequence: a), c) OCP (1200 s) – polarization at −0.5 V (1200 s) – OCP (1200 s); b), d) OCP (1200 s)– polarization at −0.5 V (1200 s) – OCP (72 h).

36]. Approximately 600 s of polarization were needed to invert this relationship. The lowest dissolution rate observed for −1 V during longer polarization could be related to the more intense reduction of H_2O_2 to H_2O, which makes the electrolyte less aggressive. This also explains the noticeable increase of ν_{Ti} immediately after coming back from −1 V to steady-state conditions (Table 2, Fig. 3). As AESEC experiments are performed in a flowing electrolyte, it can be expected that concentration of H_2O_2 in the fluid contacting with surface at the steady-state conditions would be higher than during cathodic polarization owing to suppression of its reduction at OCP. Although after polarization at −0.5 V or below, ν_{Ti} was progressively decreasing with the time of OCP monitoring, the final registered value was still significantly greater than before the polarization test (Fig. 3). Our results clearly show that cathodic polarization can induce changes in the oxide layer and indicate that accelerated ν_{Ti} can be expected not only during cathodic polarization but also at least for several minutes after completing this event. In addition to the cathodic dissolution of Ti-6Al-4V, as considered in this article, cathodic polarization may also induce hydrogen embrittlement [37]. At pH=7.4, used in this work, hydrogen evolution is thermodynamically possible whenever the potential drops below −0.5 V vs. SHE (-0.74 V vs. SCE) [38,39]. Adsorbed atomic hydrogen is formed on the surface as an intermediate in hydrogen evolution and may subsequently be absorbed in the alloy leading to a loss of ductility. Generally for Ti-6Al-4V hydrogen solubility is higher in β phase and the formation of hydrides [39] is facilitated in alloys rich in the α phase, as in our study [40]. Previous studies revealed that the brittle titanium hydride layer can be formed only when cathodic polarization is performed in fluid with pH <6, lower than in our study [41]

Applied value of cathodic potential influences not only the level and characteristic of titanium but also vanadium dissolution (Fig. 5). The most noticeable vanadium dissolution was found for the same potential as for titanium (-0.5 V). Virtually the same position of vanadium and titanium dissolution peaks (Fig. 3, Fig. 5) suggests that degradation of vanadium-rich β-phase during cathodic process was more pronounced compared to α-phase which is stabilized by aluminum. Moreover, correlating of j_V and j_{Ti} to the stoichiometry of the alloy revealed noticeably preferential dissolution of vanadium. AESEC tests did not reveal the behavior of Al, which makes difficulties in comparing behavior of Al-rich and V-rich phases. However, preferential dissolution of β-phase was confirmed by SEM observations of Ti-6Al-4V surfaces performed after completing corrosion experiments conducted in the flowing system. Additionally, prolonged exposure of previously polarized sample to PBS+H_2O_2 facilitated the corrosion of vanadium-rich phase, which was initiated by a short polarization event (Fig. 7, Fig. 8). TEM observations of a surface cross-section revealed that the oxide layer formed on α phase grains is thicker and less homogenous than those formed on the β phase (Fig. 8). EDS analysis showed that the outermost part of the oxide film was enriched in aluminum. Surprisingly, aluminum was deposited on the surfaces of grains originated from both phases (Fig. 9). These conclusions agree with XPS results reported by Hedberg et.al [42], who also found enrichment in aluminum within Ti-6Al-4V oxide film after immersion in PBS+H_2O_2. An excessive amount of aluminum in the outermost part of the oxide has been detected not only for Ti-6Al-4V exposed to the corrosion solutions but also for the spontaneously air-formed oxides that did not have prior contact with an electrolyte [43–45]. This would suggest that Al is oxidized preferentially, and when the concentration of metallic Al in the subsurface region of the alloy is decreased, Ti oxide should start to grow at the metal/oxide interface. Likewise, the cathodic polarization in PBS+H_2O_2 would result in an increase of the pH near the surface, if the generated hydroxide overtook the buffer capacity of the electrolyte. This alkalinization of the interface would in turn induce the dissolution of Al of the α phase which could precipitate on the whole surface, including β phase grains, as the electrolyte is neutralized after release of the cathodic polarization. This could explain a visibly higher concentration of Al on the top of the oxide film (Fig. 9) although further investigations are needed to clarify the origin.

Overall AESEC and microscopy results indicate that the cathodic polarization event induced corrosion of Ti-6Al-4V within both α and β phases with the most preferential dissolution of the latter one. This was confirmed by the extensive selective dissolution of β phase directly after cathodic polarization observed in the SEM micrographs (Fig. 7). Subsequent, prolonged exposure to PBS+H_2O_2 fluid under steady-state conditions resulted in further dissolution of β phase (Fig. 7). The selective dissolution of the β phase in H_2O_2 solution has been described in the literature [11,19,43,46] and a surface modification method based on this phenomenon has been patented [47]. However, little attention has been paid to the possible origin of this phenomenon. Differences in the

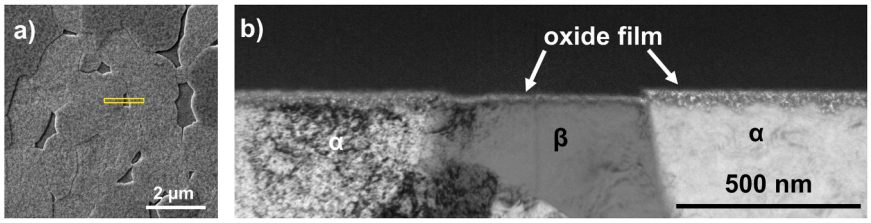

Fig. 8. Top-view and cross-section images of Ti-6Al-4V surface after following tests: OCP (1200 s) – polarization at −0.5 V– OCP (72 h). Yellow rectangle in SEM micrograph (Fig. 8a) correspond to area presented in TEM figure (Fig. 8b).

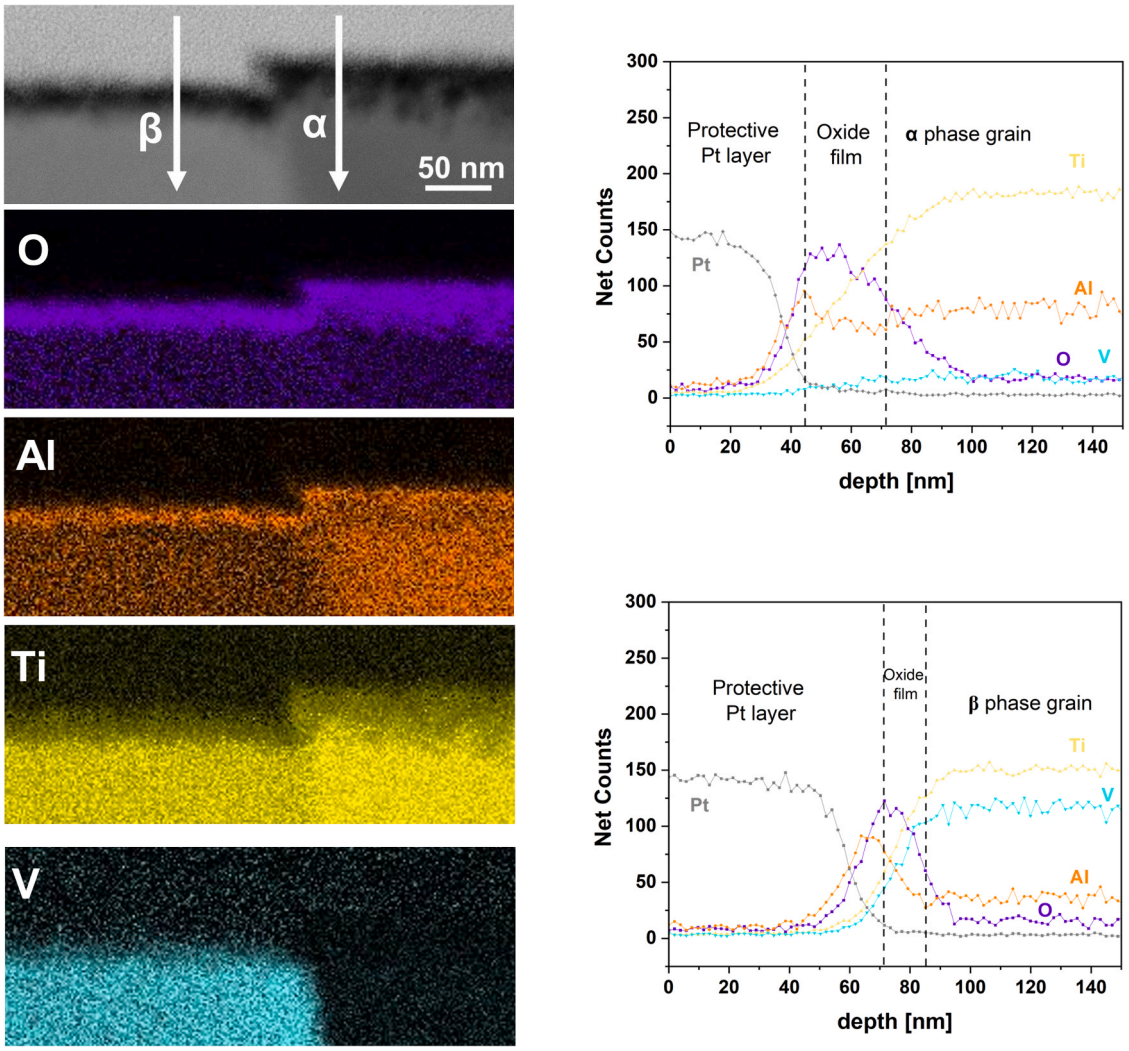

Fig. 9. EDS maps and linear scans presented elemental distribution on the cross-section of Ti-6Al-4V surface after following tests: OCP (1200 s) – polarization at −0.5 V (1200 s) – OCP (72 h). Yellow arrows visible in TEM micrographs represent direction of linear analysis.

corrosion behavior of the α and β phases may be correlated to their different crystal structures (HCP and BCC) [48] and their chemical compositions (Al-rich and V-rich), which in turn can lead to galvanic corrosion and selective dissolution of the more active phase [49,50]. Al (III) oxide or hydroxide are thermodynamically the most stable species in the pH and potential range relevant to our study [51] which would enhance the passivity of the α phase in PBS+H_2O_2 solution (pH=7.4). On the other hand, vanadium, which stabilizes the β phase, offers limited corrosion protection in physiological solutions and can be soluble as $VO_2(OH_2)^-$ [19,52] in PBS+H_2O_2 (pH=7.4) at potentials higher than approx. -0.1 V vs. SCE. This can be associated with increase the defectiveness of the oxide formed on β phase grains leading to its accelerated corrosion [36]. It follows that the selective β dissolution, activated by the cathodic potential (Fig. 7a, Fig. 7c) [47], further progresses during 72 h of immersion at the open circuit potential (Fig. 7b, Fig. 7d).

Summing up, this work for the first time demonstrates the constantly changing nature of titanium dissolution rate during cathodic polarization, which characteristic is related to the value of applied potential. Overall the results indicate that titanium dissolution during cathodic process under inflammatory conditions depends on the rapid weakening of the oxide as well as on the progressive decrease of the H_2O_2 concentration. The combination of these two factors can explain the observed non-linear dissolution vs. time relationship. These results highlight the importance of considering both potential and time of a corrosion test for predicting the effect of cathodic polarization on Ti-6Al-4V corrosion properties.

5. Conclusions

In this work we presented how the titanium dissolution rate is enhanced by the cathodic polarization conditions that may arise *in vivo* during MACC events for Ti-6Al-4V hip replacements. Performed investigation allow driving following conclusions:

- Cathodic polarization had deleterious effect on titanium dissolution only when the electrochemical process was conducted in the simulated inflammatory fluid (PBS+H_2O_2) with potential −0.5 V vs. SCE or below.
- AESEC studies revealed changing nature of dissolution rate during the time of polarization in PBS+H_2O_2 at −0.5 V vs. SCE or below. When the polarization time did not exceed 60 s, the highest dissolution was observed for the lowest potential (-1 V). When the polarization time was longer than several minutes, higher dissolution was registered at higher potential.
- Relation between applied cathodic potential and maximum dissolution rate was non-linear. AESEC results revealed that the highest dissolution can be achieved not for the lowest clinically relevant

potential (-1 V) but for intermediate cathodic potential (-0.5 V). As extensive dissolution can induce further inflammatory reaction, discovering what extent of polarization should induce the highest level of released corrosion products is important in terms predicting corrosion *in vivo*.

- Single, relatively short polarization at −0.5 V induced selective degradation of vanadium-rich β phase. Further, prolonged exposure of previously polarized Ti-6Al-4V to the PBS+H_2O_2 magnified the β phase degradation. Moreover after cathodic polarization and further immersion at steady-state conditions, Al enrichment was found on the outermost part of the oxide formed on both α and β grains.

CRediT authorship contribution statement

Kevin Ogle: Writing – original draft, Validation, Supervision, Resources, Methodology, Formal analysis, Data curation. **Fan Sun:** Writing – review & editing, Supervision, Resources, Formal analysis. **Damian Kalita:** Visualization, Methodology, Investigation, Formal analysis. **Junhui Tang:** Methodology, Investigation. **Halina Garbacz:** Writing – review & editing, Resources, Formal analysis. **Witold Chromiński:** Visualization, Methodology, Investigation, Data curation. **Agata Sotniczuk:** Writing – original draft, Visualization, Project administration, Methodology, Investigation, Funding acquisition, Formal analysis, Data curation, Conceptualization. **Chenyang Xie:** Methodology, Investigation. **Baojie Dou:** Writing – review & editing, Methodology, Investigation.

Declaration of Competing Interest

The authors declare that they have no known competing financial interests or personal relationships that could have appeared to influence the work reported in this paper.

Data availability

Data will be made available on request.

Acknowledgments

This research was funded in whole by National Science Centre, Poland within Sonatina 7 grant [2023/48/C/ST11/00085]. For the purpose of Open Access, the author has applied a CC-BY public copyright licence to any Author Accepted Manuscript (AAM) version arising from this submission.

D.K. and W.C. were financed by through the European Union Horizon 2020 research and innovation program under Grant Agreement No. 857470 and from the European Regional Development Fund of the Foundation for Polish Science International Research Agenda PLUS program Grant No. MAB PLUS/2018/8 and the initiative of the Ministry of Science and Higher Education 'Support for the activities of Centers of Excellence established in Poland under the Horizon 2020 program' under agreement No. MEiN/2023/DIR/3795.

References

[1] S. Balachandran, Z. Zachariah, A. Fischer, D. Mayweg, M.A. Wimmer, D. Raabe, M. Herbig, Atomic scale origin of metal ion release from hip implant taper junctions, Adv. Sci. 7 (2020) 1903008, https://doi.org/10.1002/advs.201903008.

[2] L. Kunčická, R. Kocich, T.C. Lowe, Advances in metals and alloys for joint replacement, Prog. Mater. Sci. 88 (2017) 232–280, https://doi.org/10.1016/j.pmatsci.2017.04.002.

[3] M. Geetha, A.K. Singh, R. Asokamani, A.K. Gogia, Ti based biomaterials, the ultimate choice for orthopaedic implants – a review, Prog. Mater. Sci. 54 (2009) 397–425, https://doi.org/10.1016/j.pmatsci.2008.06.004.

[4] J. Capek, M. Sepúlveda, J. Bacova, J. Rodriguez-Pereira, R. Zazpe, V. Cicmancova, P. Nyvltova, J. Handl, P. Knotek, K. Baishya, Ultrathin TiO2 coatings via atomic layer deposition strongly improve cellular interactions on planar and nanotubular biomedical Ti substrates, ACS Appl. Mater. Interfaces (2024), https://doi.org/10.1021/acsami.3c17074.

[5] J.L. Gilbert, Corrosion in the human body: metallic implants in the complex body environment, Corrosion 73 (2017) 1478–1495, https://doi.org/10.5006/2563.

[6] F. Yu, O. Addison, A.J. Davenport, A synergistic effect of albumin and H2O2 accelerates corrosion of Ti6Al4V, Acta Biomater. 26 (2015) 355–365, https://doi.org/10.1016/j.actbio.2015.07.046.

[7] Y. Bao, A.I. Munoz, B.M. Jolles, S. Mischler, Assessment of in-vivo corrosion of Ti and CoCrMo joint implants by electrochemical measurements in human synovial liquids, Electrochim. Acta 476 (2024) 143708, https://doi.org/10.1016/j.electacta.2023.143708.

[8] J.-L. Wang, R.L. Liu, T. Majumdar, S.A. Mantri, V.A. Ravi, R. Banerjee, N. Birbilis, A closer look at the in vitro electrochemical characterisation of titanium alloys for biomedical applications using in-situ methods, Acta Biomater. 54 (2017) 469–478, https://doi.org/10.1016/j.actbio.2017.03.022.

[9] D.C. Rodrigues, P. Valderrama, T.G. Wilson, Jr, K. Palmer, A. Thomas, S. Sridhar, A. Adapalli, M. Burbano, C. Wadhwani, Titanium corrosion mechanisms in the oral environment: a retrieval study, Materials 6 (2013) 5258–5274, https://doi.org/10.3390/ma6115258.

[10] J.L. Gilbert, S. Mali, R.M. Urban, C.D. Silverton, J.J. Jacobs, In vivo oxide-induced stress corrosion cracking of Ti-6Al-4V in a neck–stem modular taper: emergent behavior in a new mechanism of in vivo corrosion, J. Biomed. Mater. Res. Part B Appl. Biomater. 100 (2012) 584–594, https://doi.org/10.1002/jbm.b.31943.

[11] M.A. Kurtz, P. Khullar, J.L. Gilbert, Cathodic activation and inflammatory species are critical to simulating in vivo Ti-6Al-4V selective dissolution, Acta Biomater. 149 (2022) 399–409, https://doi.org/10.1016/j.actbio.2022.07.020.

[12] J.C.H. Carlson, D.W. Van Citters, J.H. Currier, A.M. Bryant, M.B. Mayor, J. P. Collier, Femoral stem fracture and in vivo corrosion of retrieved modular femoral hips, J. Arthroplast. 27 (2012) 1389–1396, https://doi.org/10.1302/0301-620X.76B1.8300685.

[13] S.D. Cook, R.L. Barrack, A.J. Clemow, Corrosion and wear at the modular interface of uncemented femoral stems, J. Bone Jt. Surg. Br. Vol. 76 (1994) 68–72, https://doi.org/10.1302/0301-620X.76B1.8300685.

[14] Y. Liu, D. Zhu, D. Pierre, J.L. Gilbert, Fretting initiated crevice corrosion of 316LVM stainless steel in physiological phosphate buffered saline: potential and cycles to initiation, Acta Biomater. 97 (2019) 565–577, https://doi.org/10.1016/j.actbio.2019.07.051.

[15] Y. Xu, J. Qi, J. Nutter, J. Sharp, M. Bai, L. Ma, W.M. Rainforth, Correlation between the formation of tribofilm and repassivation in biomedical titanium alloys during tribocorrosion, Tribol. Int. 163 (2021) 107147, https://doi.org/10.1016/j.triboint.2021.107147.

[16] V. Swaminathan, J.L. Gilbert, Potential and frequency effects on fretting corrosion of Ti6Al4V and CoCrMo surfaces, J. Biomed. Mater. Res. Part A. 101 (2013) 2602–2612, https://doi.org/10.1002/jbm.a.34564.

[17] M.A. Kurtz, K. Alaniz, L.M. Taylor, A. Moreno-Reyes, J.L. Gilbert, Increasing temperature accelerates Ti-6Al-4V oxide degradation and selective dissolution: an arrhenius-based analysis, Acta Biomater. (2024), https://doi.org/10.1016/j.actbio.2024.02.028.

[18] E. Brooks, M. Tobias, K. Krautsak, M. Ehrensberger, The influence of cathodic polarization and simulated inflammation on titanium electrochemistry, J. Biomed. Mater. Res. Part B Appl. Biomater. 102 (2014) 1445–1453, https://doi.org/10.1002/jbm.b.33123.

[19] M. Prestat, F. Vucko, L. Holzer, D. Thierry, Microstructural aspects of Ti6Al4V degradation in H2O2-containing phosphate buffered saline, Corros. Sci. (2021) 109640, https://doi.org/10.1016/j.corsci.2021.109640.

[20] Y. Zhang, O. Addison, F. Yu, B.C.R. Troconis, J.R. Scully, A.J. Davenport, Time-dependent enhanced corrosion of Ti6Al4V in the presence of H2O2 and albumin, Sci. Rep. 8 (2018) 3185, https://doi.org/10.1038/s41598-018-21332-x.

[21] M. Prestat, D. Thierry, Corrosion of titanium under simulated inflammation conditions: clinical context and in vitro investigations, Acta Biomater. 136 (2021) 72–87, https://doi.org/10.1016/j.actbio.2021.10.002.

[22] A. Sotniczuk, J.L. Gilbert, Y. Liu, M. Matczuk, W. Chromiński, D. Kalita, M. Pisarek, H. Garbacz, Corrosion resistance of β-phase titanium alloys under simulated inflammatory conditions: exploring the relevance of biocompatible alloying elements, Corros. Sci. 220 (2023) 111271, https://doi.org/10.1016/j.corsci.2023.111271.

[23] J.L. Gilbert, G.W. Kubacki, Oxidative Stress, Inflammation, and the Corrosion of Metallic Biomaterials: Corrosion Causes Biology and Biology Causes Corrosion, in: Oxidative Stress Biomater, Elsevier, 2016, pp. 59–88, https://doi.org/10.1016/B978-0-12-803269-5.00003-6.

[24] M.A. Kurtz, R. Yang, D. Liu, M.S.R. Elapolu, R. Rai, J.L. Gilbert, Deep neural network predicts Ti-6Al-4V dissolution state using near-field impedance spectra, Adv. Funct. Mater. 34 (2024) 2308932, https://doi.org/10.1002/adfm.202308932.

[25] K. Ogle, Atomic emission spectroelectrochemistry: real-time rate measurements of dissolution, corrosion, and passivation, Corrosion 75 (2019) 1398–1419, https://doi.org/10.5006/3336.

[26] K. Ogle, S. Weber, Anodic dissolution of 304 stainless steel using atomic emission spectroelectrochemistry, J. Electrochem. Soc. 147 (2000) 1770, https://doi.org/10.1149/1.1393433.

[27] K. Ogle, M. Serdechnova, M. Mokaddem, P. Volovitch, The cathodic dissolution of Al, Al2Cu, and Al alloys, Electrochim. Acta 56 (2011) 1711–1718, https://doi.org/10.1016/j.electacta.2010.09.058.

[28] B. Laurent, N. Gruet, B. Gwinner, F. Miserque, M. Tabarant, K. Ogle, A direct measurement of the activation potential of stainless steels in nitric acid, J. Electrochem. Soc. 164 (2017) C481–C487, https://doi.org/10.1149/2.0081709jes.

[29] ASTM International, ASTM B348 Standard Specification for Titanium and Titanium Alloy Bars and Billets, 2010.
[30] M.A. Kurtz, A.C. Wessinger, A. Mace, A. Moreno-Reyes, J.L. Gilbert, Additively manufactured Ti-29Nb-21Zr shows improved oxide polarization resistance versus Ti-6Al-4V in inflammatory simulating solution, J. Biomed. Mater. Res. Part A. (2023), https://doi.org/10.1002/jbm.a.37552.
[31] X.-R. Li, X.-Z. Meng, Q.-H. Zhang, L.-K. Wu, Q.-Q. Sun, H.-Q. Deng, S.-J. Sun, F.-H. Cao, Insight into oxygen reduction activity and pathway on pure titanium using scanning electrochemical microscopy and theoretical calculations, J. Colloid Interface Sci. 643 (2023) 551–562, https://doi.org/10.1016/j.jcis.2023.03.127.
[32] X.-R. Li, Q.-H. Zhang, X.-Z. Meng, L.-K. Wu, F.-H. Cao, Effect of pretreatments on the hydrogen evolution kinetics of pure titanium using impedance and SECM technologies, Corros. Sci. 191 (2021) 109726, https://doi.org/10.1016/j.corsci.2021.109726.
[33] J. Pan, D. Thierry, C. Leygraf, Electrochemical and XPS studies of titanium for biomaterial applications with respect to the effect of hydrogen peroxide, J. Biomed. Mater. Res. 28 (1994) 113–122, https://doi.org/10.1002/jbm.820280115.
[34] M.A. Kurtz, A.C. Wessinger, L.M. Taylor, J.L. Gilbert, Electrode potential, inflammatory solution chemistry and temperature alter Ti-6Al-4V oxide film properties, Electrochim. Acta (2023) 142770, https://doi.org/10.1016/j.electacta.2023.142770.
[35] P. Tengvall, I. Lundström, Physico-chemical considerations of titanium as a biomaterial, Clin. Mater. 9 (1992) 115–134, https://doi.org/10.1016/0267-6605(92)90056-Y.
[36] M. Metikos-Huković, A. Kwokal, J. Piljac, The influence of niobium and vanadium on passivity of titanium-based implants in physiological solution, Biomaterials 24 (2003) 3765–3775, https://doi.org/10.1016/S0142-9612(03)00252-7.
[37] T. Ohtsuka, M. Masuda, N. Sato, Cathodic reduction of anodic oxide films formed on titanium, J. Electrochem. Soc. 134 (1987) 2406, https://doi.org/10.1149/1.2100212.
[38] P. Acevedo-Peña, J. Vazquez-Arenas, R. Cabrera-Sierra, L. Lartundo-Rojas, I. González, Ti Anodization in alkaline electrolyte: the relationship between transport of defects, film hydration and composition, J. Electrochem. Soc. 160 (2013) C277, https://doi.org/10.1149/2.063306jes.
[39] Q. Yin, S. Liu, X.-Z. Fu, X.-Z. Wang, J.-L. Luo, Transition of self-passivation and semiconductor property of titanium in the simulated environments of proton exchange membrane fuel cells, Appl. Surf. Sci. 612 (2023) 155930, https://doi.org/10.1016/j.apsusc.2022.155930.
[40] P. Metalnikov, D. Eliezer, G. Ben-Hamu, E. Tal-Gutelmacher, Y. Gelbstein, C. Munteanu, Hydrogen embrittlement of electron beam melted Ti–6Al–4V, J. Mater. Res. Technol. 9 (2020) 16126–16134, https://doi.org/10.1016/j.jmrt.2020.11.073.
[41] K. Videm, S. Lamolle, M. Monjo, J.E. Ellingsen, S.P. Lyngstadaas, H.J. Haugen, Hydride formation on titanium surfaces by cathodic polarization, Appl. Surf. Sci. 255 (2008) 3011–3015, https://doi.org/10.1016/j.apsusc.2008.08.090.
[42] Y.S. Hedberg, M. Žnidaršič, G. Herting, I. Milošev, I. Odnevall Wallinder, Mechanistic insight on the combined effect of albumin and hydrogen peroxide on surface oxide composition and extent of metal release from Ti6Al4V, J. Biomed. Mater. Res. Part B Appl. Biomater. 107 (2019) 858–867, https://doi.org/10.1002/jbm.b.34182.
[43] S. Höhn, S. Virtanen, Effect of inflammatory conditions and H2O2 on bare and coated Ti–6Al–4V surfaces: corrosion behavior, metal ion release and Ca-P formation under long-term immersion in DMEM, Appl. Surf. Sci. 357 (2015) 101–111, https://doi.org/10.1016/j.apsusc.2015.08.261.
[44] D.M. Brunette, P. Tengvall, M. Textor, P. Thomsen, Titanium in Medicine: Material Science, Surface Science, Engineering, Biological Responses and Medical Applications, Springer Science & Business Media, 2012.
[45] I. Milošev, M. Metikoš-Huković, H.-H. Strehblow, Passive film on orthopaedic TiAlV alloy formed in physiological solution investigated by X-ray photoelectron spectroscopy, Biomaterials 21 (2000) 2103–2113, https://doi.org/10.1016/S0142-9612(00)00145-9.
[46] S. Höhn, A. Braem, B. Neirinck, S. Virtanen, Albumin coatings by alternating current electrophoretic deposition for improving corrosion resistance and bioactivity of titanium implants, Mater. Sci. Eng. C 73 (2017) 798–807, https://doi.org/10.1016/j.msec.2016.12.129.
[47] J. Gilbert, Z. Bai, N. Chandrasekaran, Method for preparing biomedical surfaces, (2011).
[48] L. Deconinck, M.T. Villa Vidaller, E. Bernardo Quejido, E.A. Jägle, T. Depover, K. Verbeken, In-situ hydrogen embrittlement evaluation of as-built and heat treated laser powder bed fused Ti-6Al-4V versus conventionally cold rolled Ti-6Al-4V, Addit. Manuf. 76 (2023) 103768, https://doi.org/10.1016/j.addma.2023.103768.
[49] H. Zhang, C. Man, L. Wang, C. Dong, L. Wang, D. Kong, X. Wang, Different corrosion behaviors between α and β phases of Ti6Al4V in fluoride-containing solutions: influence of alloying element Al, Corros. Sci. 169 (2020) 108605, https://doi.org/10.1016/j.corsci.2020.108605.
[50] J.-R. Chen, W.-T. Tsai, In situ corrosion monitoring of Ti–6Al–4V alloy in H2SO4/HCl mixed solution using electrochemical AFM, Electrochim. Acta 56 (2011) 1746–1751, https://doi.org/10.1016/j.electacta.2010.10.024.
[51] O.M. Leung, T. Schoetz, T. Prodromakis, C. Ponce de Leon, Review—progress in electrolytes for rechargeable aluminium batteries, J. Electrochem. Soc. 168 (2021) 56509, https://doi.org/10.1149/1945-7111/abfb36.
[52] M. Pourbaix, Atlas of electrochemical equilibria in aqueous solutions, NACE. (1966).